Coarse-grained simulations of moderately entangled star polyethylene melts

L. Liu,[1] J. T. Padding,[2] W. K. den Otter,[1] and W. J. Briels[1,a)]
[1]*Computational Biophysics, MESA+, University of Twente, P.O. Box 217, 7500 AE Enschede, The Netherlands*
[2]*Department of Chemical Engineering and Chemistry, Eindhoven University of Technology, P.O. Box 513, 5600 MB Eindhoven, The Netherlands*

(Received 6 February 2013; accepted 7 June 2013; published online 28 June 2013)

In this paper, a previous coarse-grain model [J. T. Padding and W. J. Briels, J. Chem. Phys. **117**, 925 (2002)] to simulate melts of linear polymers has been adapted to simulate polymers with more complex hierarchies. Bond crossings between highly coarse-grained soft particles are prevented by applying an entanglement algorithm. We first test our method on a virtual branch point inside a linear chain to make sure it works effectively when linking two linear arms. Next, we apply our method to study the diffusive and rheological behaviors of a melt of three-armed stars. We find that the diffusive behavior of the three-armed star is very close to that of a linear polymer with the same molecular weight, while its rheological properties are close to those of a linear chain with molecular mass equal to that of the longest linear sub-chain in the star. © *2013 AIP Publishing LLC*. [http://dx.doi.org/10.1063/1.4811675]

I. INTRODUCTION

Polyethylene is among the most important commercial plastics with a variety of applications in our daily lives, such as films, extrusion coating, food packaging.[1] It can be produced in a variety of different forms based on two main structural types: high density linear polyethylene and low density branched polyethylene. It has been found that the properties of polymer melts depend sensitively on the details of the chain architecture.[2–12] Thus to have a good understanding of the properties of polymers in relation to the various possible topologies would be of great use to optimize the processing and synthesis techniques from both industrial and scientific perspectives.

The dynamical and rheological properties of linear polymer systems are described quite well by the Rouse model for short chains[13] and the reptation model for entangled chains.[14] The experimentally observed scaling laws for the melt self-diffusion coefficient and viscosity as a function of molecular weight are explained successfully by these models.[15–17] Besides this, computational methods have been developed to test theoretical predictions and reveal new phenomena along with experiments in this field.

Among the computer simulations, fully atomistic molecular simulations are usually carried out to acquire accurate fundamental information on polymer structures and dynamics in relation to their chemical details.[18–22] However, with current computer capabilities these goals become unaccomplishable with highly entangled systems, where long relaxation times and large simulation boxes have to be dealt with. In cases when less detailed information is needed to understand the basic physical phenomena of interest, coarse-graining techniques offer an alternative and efficient way to reach long time and length scales. For example, when studying the flow properties of linear polymers, one is mainly interested in some generic properties of entire chains.[23–28]

Despite the advantages of coarse-grain simulations, one should be aware of the fact that the coarse-grain potential will become increasingly softer on lumping more and more atoms together, and consequently bonds will finally be capable of crossing each other. Such illegal bond crossings may be prevented by a number of uncrossability constraints. One has been developed by Padding and Briels in a method, called TWENTANGLEMENT, based on introducing an "entanglement" at the touching location of two elastic bonds.[25] During the remaining part of the run, the entanglement points are updated with every time step by minimizing the elastic energy in the two entangled bonds, until they disentangle again. This model has been shown to be able to describe the effects of entanglements and to reproduce effectively experimental data of moderately entangled linear polymer melts.[26]

In this work, we extend the program to be applicable to architecturally complex systems. Roughly speaking, we have updated the entanglement algorithm to prevent crossings between all branches of all polymers. Star polymers with a single branch point architecture presents the simplest example of a branched polymer, and have attracted scientific interests for a long time.[29–34] We therefore first apply our model on star polymers.

The organization of this paper is as follows: in Sec. II, we describe the coarse-grained simulation model and introduce the uncrossability constraint. The topology specification is also discussed in this part. In Sec. III, the properties of star polymer are presented and we make the comparisons between 3-arm star and linear chains. Section IV contains the conclusions of this work.

a)w.j.briels@utwente.nl

II. MODEL OVERVIEW AND SIMULATED SYSTEMS

A. Coarse-graining method and Brownian dynamics

Considering that the chemical details are unimportant when studying the dynamical properties of polymers at large time and length scales, we group a large number, $\lambda = 20$, of monomers together into one coarse-grained bead (also referred to as blob). Accordingly, a coarse-grained chain can be described by several consecutive blobs. For example, a linear polyethylene chain $C_{140}H_{282}$ in this work is represented by seven blobs and named B_7.

For each blob, the center of mass position $\mathbf{R}$ is the average of λ monomer locations $\mathbf{r}_i$, which are weighted by their mass m_i,

$$\mathbf{R} = \frac{1}{M}\sum_{i=1}^{\lambda} m_i \mathbf{r}_i, \tag{1}$$

where M is the blob's total mass. Blobs are simply treated as Brownian particles and their center of mass positions are evolving through a time dependent first-order Langevin equation, which includes displacements due to forces and random displacements $\delta\mathbf{R}_i$,

$$d\mathbf{R}_i = -\frac{1}{\xi}\nabla_i \Phi dt + \delta\mathbf{R}_i, \tag{2}$$

where Φ is the potential energy and ξ is the blob friction coefficient. We assume that the friction coefficients are independent of the blob configurations, and are related to the stochastic displacements through the fluctuation-dissipation theorem

$$\langle \delta R_{i\alpha} \cdot \delta R_{j\beta} \rangle = \frac{2k_B T}{\xi} dt \delta_{ij}\delta_{\alpha\beta}, \tag{3}$$

where Greek subscripts refer to coordinate directions, k_B is Boltzmann's constant, and T is the temperature of the system.

Forces between blobs are derived from the potential of mean force, which is related to the n-blob probability distribution function P_n according to

$$\Phi(\mathbf{R}^n) = -k_B T \ln P_n(\mathbf{R}^n), \tag{4}$$

where P_n may be obtained from an appropriate atomistic simulation.

We assume that the total potential of mean force can be approximately expressed by three independent contributions: a sum over all non-bonded pairs, one over bonded blobs, and one over bond angles,

$$\Phi(\mathbf{R}^n) = \sum_{i<j} \varphi^{nb}(R_{i,j}) + \sum_i \varphi^{b}(R_{i,i+1}) + \sum_i \varphi^{\theta}(\theta_i). \tag{5}$$

The inter- and intra-molecular interactions together with potential functions are shown in Table I. A Gaussian pair potential is used to describe repulsive forces between non-bonded φ^{nb} and bonded $\varphi^{b_{rep}}$ blobs. The attractive part $\varphi^{b_{att}}$ for bonded interaction is described by a single power law. And the bending potential φ^{θ} is a cosine function of the angle θ between two consecutive bonds.

The blob interactions are of course more complicated than assumed here. However, it is known that entanglement effects play a dominant role in the rheology of polymeric systems. This allows us to neglect to a large extent all details of the interactions in our simulation work. Similar assumptions are made in several other rheological simulation methods like in the works of the Naples group,[35–37] and in the work of Schieber,[38,39] and Likhtman.[40–42] All these entanglement-based methods have the drawback that the diagonal elements of the stress tensor are not necessarily correct and that thermodynamic properties in general are not described at all. A coarse-grain model that does describe both thermodynamics and rheology correctly was introduced by our group some time ago and now goes with the name RaPiD.[43–47] This model, however, does not explicitly include the architectural issues that we want to address in this paper.

TABLE I. Interactions between non-bonded and bonded blobs.

Interaction type	Potential expression
Non-bonded	$\varphi^{nb}(R) = c_0 e^{-(R/b_0)^2}$
Bonded repulsive	$\varphi^{b_{rep}}(R) = c_1 e^{-(R/b_1)^2} + c_2 e^{-(R/b_2)^2}$
Bonded attractive	$\varphi^{b_{att}}(R) = c_3 (R)^{\mu}$
Bending potential	$\varphi^{\theta}(\theta) = c_4(1+\cos\theta)^{v}$

B. Uncrossability constraint

As mentioned in Sec. II A, every 20 monomer units are lumped together to form a highly coarse-grained particle. Due to the high coarse-graining level, the interaction potential of blobs becomes very soft and bonds can cross each other. In order to prevent the occurrence of this kind of unrealistic phenomenon, we implement an uncrossability constraint algorithm (see below), which introduces entanglements when imminent bond crossings are detected. The number of monomers mapped on one blob on the one hand satisfies the need for a large integration time step, and on the other hand assures that the size of the blobs is smaller than one reptation tube diameter. This allows for the possibility of reptation to emerge from the simulation. A coarse graining to blobs larger than the tube diameter will smear out confinement effects, resulting from the potential interactions and the imposed uncrossability constraints, and show reptation at an incorrect length scale, unless reptational moves are introduced by hand at the level of the blobs.

The uncrossability constraint is based on the consideration that bonds between blobs have elastic properties. By means of a geometric check, as soon as two bonds are detected to touch each other, an entanglement point $\mathbf{X}$ will be created at the crossing site. Concomitantly, the attractive potential contributed by the two crossing bonds is changed by replacing the two blob distances $R_{i,i+1}$ by pathlengths $L_{i,i+1}$,

$$\varphi^{att}(L_{i,i+1}) = c_3 (L_{i,i+1})^{\mu}. \tag{6}$$

The pathlength $L_{i,i+1}$ is the contourlength of the path that starts at blob i and goes via a number of entanglement points $\mathbf{X}_1, \mathbf{X}_2, \ldots, \mathbf{X}_p$, to the next blob $i+1$,

$$L_{i,i+1} = |\mathbf{R}_i - \mathbf{X}_1| + |\mathbf{X}_1 - \mathbf{X}_2| + \cdots + |\mathbf{X}_{p-1} - \mathbf{X}_p| + |\mathbf{X}_p - \mathbf{R}_{i+1}|. \tag{7}$$

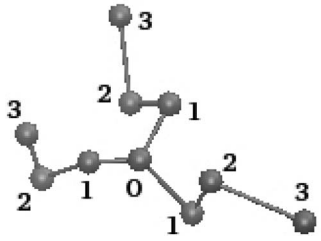

FIG. 1. Schematic representation of $B(B_3)_2$ with a branch point and three arms.

With every time step the "entanglements" so created are updated such as to minimize the total attractive bond energy, and thereby forbid chain crossing. We stress that the number of entanglements so defined is not the same as the entanglement number **Z** as it is used in reptation theory. It is rather the long-lasting entanglements which define the entanglement number. We refer to the original paper by Padding and Briels[26] for a distribution of entanglement lifetimes for the linear chains.

C. Topology specification and simulation details

We conduct our simulations with linear and star polyethylene melts at a temperature of 450 K. The numberings of a 3-arm star polymer are shown in Fig. 1. The name of a star polymer is defined by putting information of the branch point into the first bracket, and after that the length and number of star arms. For example, $B(B_3)_3$ consists of one branch point to which three arms are attached, each consisting of three blobs. Linear chains of n blobs in this scheme are simply called B_n. Notice that the properties of, for example, B_7 and $B(B_3)_2$ should be the same.

The main complication with the simulation of star polymers is due to the presence of a branch point. In this paper, we build stars by linking together linear chains to one central branch point. Any two linear chains connected at a branch point should then communicate through appropriate potential forces not present before the connection. Moreover, entanglements should be dealt with correctly.

In view of the algorithmic complications, we first implemented a simple test to ensure that a branch point works properly when linking together two linear chains. The general idea is displayed in Fig. 2, where two B_4 chains are connected at a branch point by overlapping the tail and head blob of the first and second B_4 chains. Consequently, a new chain, called

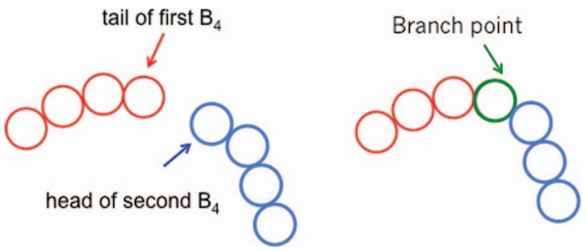

FIG. 2. Sketch of $B(B_3)_2$ on the right with a branch point made by joining two B_4 chains on the left.

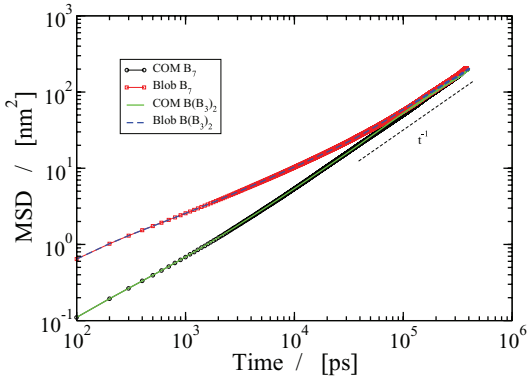

FIG. 3. Diffusion of B_7 and $B(B_3)_2$. For both center of mass and blobs, these two chains diffuse in the same way.

$B(B_3)_2$ with a branch point B and two side arms $(B_3)_2$, is created. We assume that the branch point has a mass and friction equal to that of a normal blob. Provided that the two originally separated B_4 chains now communicate their entanglements through the shared branch point in a correct way, the newly formed $B(B_3)_2$ should be equivalent with a single B_7 according to the effective blob number. Therefore, entanglements which slip over the branch-end of one chain should not be eliminated, as they would be at a regular end of a chain, but be recognized as entanglements at the partner chain at the other side of the branch point. Only if this is done correctly will the correct results be obtained for the longer chain. The procedure followed by us at branch points of functionality three will be described below.

Blob and center of mass mean square displacements of $B(B_3)_2$ and B_7 chains are shown in Fig. 3. The simulation parameters are given in Table II. From this plot, it is seen that the new linear chain with a branch point inside diffuses in exactly the same way as B_7. We also make a comparisons of the rheological properties of both systems expressed by their zero shear stress relaxation moduli. In Fig. 4, the shear relaxation modulus of $B(B_3)_2$ very well follows that of B_7. We conclude that the branch point works perfectly well in terms of chain dynamics.

Now shifting our attention to branch points in multi-armed stars, we need to take care that the angle between two bonds connected through a branch point should be treated

TABLE II. Parameters for potential of mean force.

Types	Parameter	Value	Unit
Non-bonded	c_0	5.56	kJ mol^{-1}
	b_0	0.49	nm
Bonded repulsive	c_1	10.46	kJ mol^{-1}
	b_1	0.26	nm
	c_2	3.49	kJ mol^{-1}
	b_2	0.67	nm
Bonded attractive	c_3	6.46	10^{-3} kJ mol^{-1} nm$^{-\mu}$
	μ	9.73	
Angular	c_4	3.01	kJ mol^{-1}
	c_5	24.08	kJ mol^{-1}
	ν	1.2	

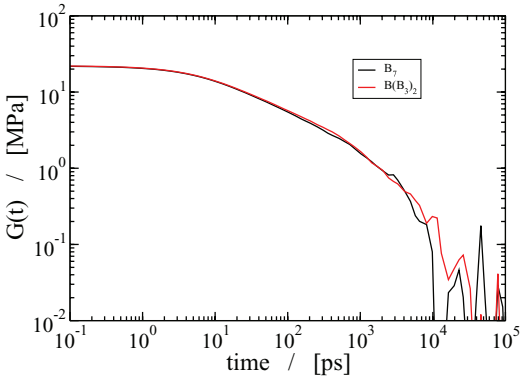

FIG. 4. Stress autocorrelation function of B_7 and $B(B_3)_2$, they are following the same relaxation behavior.

differently than the one in a linear chain. The bonds inside a linear chain form angles taking any value between zero and π. With three-armed stars we expect that the arms at the branched point will on average be co-planar and make angles of $2/3\pi$. In order to encourage our coarse-grained system to take this configuration, we have changed the bending potential at the branch point to

$$\varphi^{\theta}_{bp}(\theta) = c_5 \left(\cos\theta - \cos\frac{2}{3}\pi\right)^2. \tag{8}$$

In Fig. 5, we have plotted the observed probability distributions (pdf), both for the bond angles along the arms (panel (a)) and for those at the branch points (panel (b)), with parameters given in Table II. Notice that the pdf for the branch points has its maximum at a value of $\cos\theta$ slightly higher than -0.5, i.e., at angles slightly smaller than $2/3\pi$. The reason for this is that with non co-planer bonds the total sum of the bond angles is less than 2π.

We finally must decide what happens to entanglement that slip over the branch point. Consider an entanglement that "lives" on arm number one and slips over the branch point, as illustrated in Fig. 6. After this move the entanglement may find itself in one of four situations, it may have been annihilated, it may be entangled either with arm number two or number three, or it may be entangled with both arms number two and number three. We have implemented the following al-

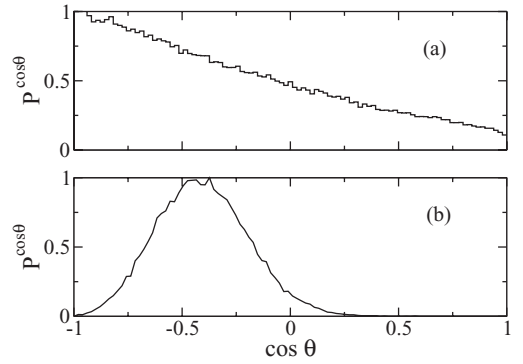

FIG. 5. Probability distributions of bending angles in arbitrary unit. Panel (a) shows the bond angles along the arms, and curve in panel (b) for those at the branch points.

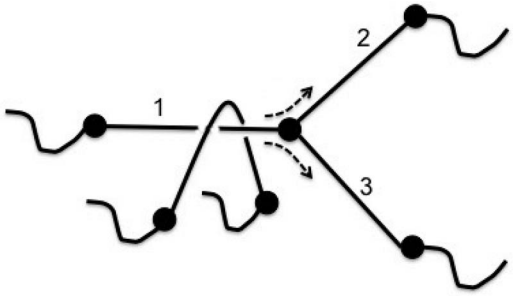

FIG. 6. Diagram of an entanglement slipping past a branch point.

gorithm. After the slip, we randomly choose either arm number two or arm number three. For the chosen arm, we perform the usual entanglement checks after a slip over a blob. If an entanglement occurs with this arm, we stick to this entanglement ignoring other possibilities. If no entanglement occurs with this arm, we perform the entanglement checks for the remaining arm. If an entanglement does occur with this arm, we stick to this one and continue the run. In case also with this arm no entanglement survives, we annihilate the entanglement and continue the run. This algorithm will give the correct result in case the entanglement is finally annihilated. In case, exactly one entanglement should remain, the algorithm will find the correct arm. In case, two entanglements should occur, the algorithm only creates one on a randomly chosen arm. A large number of geometrical checks would be required to check for double entanglements. All results with the present algorithm are therefore valid under the assumption that double entanglements are relatively rare.

To generate an equilibrated box, we randomly place a number of polymers into the simulation box, keeping the mass density equal to its melt value of $\rho = 0.761$ g/cm^3. Unentangled simulations are performed first to allow a thorough equilibration. Then the uncrossability constraints are switched on to add the entanglement effect. The parameters for the potential of mean forces of this model are shown in Table II. They apply when $\lambda = 20$, and are fit to the distribution functions obtained in atomistic simulations.[25]

III. RESULTS

In this section, we discuss typical blob time dependent mean square displacements. To this end, we number the blobs along the arms of each star from zero to three. With each star and each arm, blob number zero is the branch point and blob number three is the end point, shown in Fig. 1. Blob number one is the blob which is topologically closest to the branch point and blob number two is closest to the end point. The mean square displacement for blobs of type i is then

$$\mathbf{MSD}_i = \langle[\mathbf{R}_i(t) - \mathbf{R}_i(0)]^2\rangle, \tag{9}$$

here the pointy brackets denote the usual average over initial times and an average over all blobs of type i, i.e., over all stars and all arms. Besides these, we will also discuss the averaged blob mean square displacement, $\mathbf{MSD}_{bl} = \frac{3}{10}\sum_{i=1}^{3}\mathbf{MSD}_i + \frac{1}{10}\mathbf{MSD}_0$ and $\mathbf{MSD}_{cm} = \langle[\mathbf{R}^{cm}(t) - \mathbf{R}^{cm}(0)]^2\rangle$, with the $\mathbf{R}^{cm}$ being the center of mass of the star.

Furthermore, we will discuss the shear relaxation modulus $G(t)$, i.e., the linear stress response to a step strain. It can be measured from equilibrium fluctuations of the stress tensor as follows:

$$G(t) = \frac{V}{k_B T}\langle \sigma_{\alpha\beta}(t)\sigma_{\alpha\beta}(0)\rangle, \quad \alpha \neq \beta, \tag{10}$$

with V the total volume of the simulation box, $\alpha, \beta \in \{x, y, z\}$ are different coordinate directions, and $\sigma_{\alpha\beta}$ is the microscopic stress tensor

$$\sigma_{\alpha\beta} = -\frac{1}{V}\sum_{i,j}(r_{i,\beta} - r_{j,\beta})F_{ij,\alpha}, \tag{11}$$

where $\mathbf{r}$ is the blob position vector, and $F_{ij,\alpha}$ is the α component of the force on blob i exerted by blob j. From $G(t)$ we obtain the storage $G'(\omega)$ and loss modulus $G''(\omega)$ in the usual way

$$\begin{aligned} G'(\omega) &= \omega\int_0^\infty \sin(\omega t)G(t)dt, \\ G''(\omega) &= \omega\int_0^\infty \cos(\omega t)G(t)dt. \end{aligned} \tag{12}$$

A. Dynamics and rheological properties of star polymer

In order to confirm the complete relaxation of our stars at the longest chain length possible, we have calculated time dependent autocorrelation functions (ACF) for the unit vectors directed from the branch point to the end-points of the star arms. The results are shown in Fig. 7 below, together with those for the end-end vectors of linear chains. It is clear from this picture that, even when the decay of the branch-end vectors for our star is very slow, many decay-times fit within the total runtime 10^6 ps. We are assured, therefore, that our system is well equilibrated. Similar conclusions may be drawn from the mean-square displacements discussed next.

In Fig. 8, we display the blob and center of mass mean square displacements both when entanglements are accounted for (black curves) and when entanglements have been ignored (red curves). As is clear from the plots, entanglements

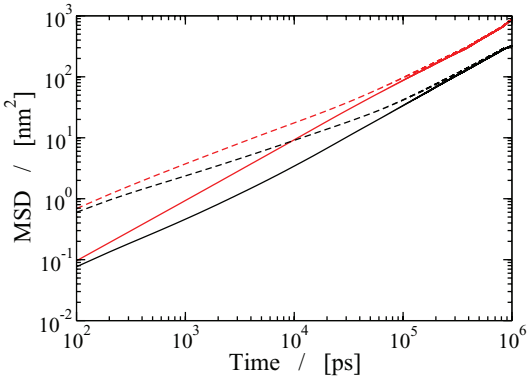

FIG. 8. Blob mean square displacement (dashed) and center of mass mean square displacement (solid) of $B(B_3)_3$ with (black) and without (red) entanglement.

substantially slow down the almost Rouse-like mean square displacements obtained for non-entangling polymers.

In order to better understand the structural diffusion of entangled stars, we have measured typical blob mean square displacements and plotted them in Fig. 9. As a result of the symmetrical arrangement of the various blobs in $B(B_3)_3$, blobs on equivalent positions along the three arms diffuse according to identical curves. The curves in Fig. 9 can therefore be separated into four groups, from bottom to top corresponding to segmental motions of the innermost branch point to the outermost free ends of each of the arms of the star. At early times, because of topological constraints originating along three different arms, the central branch point moves very slowly, in fact almost immediately as slow as in its final diffusive regime (solid black). The blobs next to the branch point move substantially faster than the branch point and become diffusive at a much later time. This trend continues with blobs being situated increasingly further outwards along the arms, with the arm end being the fastest of all, becoming diffusive only at a very late time.

In order to analyse the dynamics of the various blobs even further, we have calculated Rouse modes and their time correlation functions. In the Appendix, we shortly review the application of the Rouse model to nonlinear polymers. From a mathematical point of view, the analysis in the

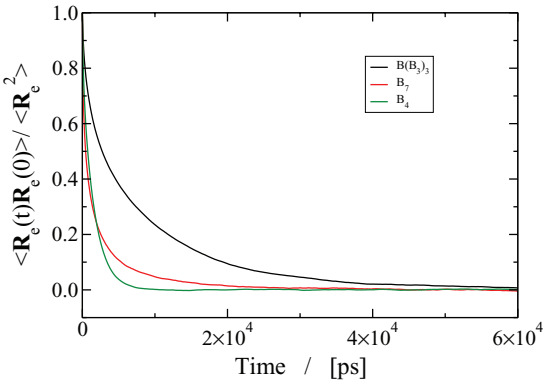

FIG. 7. Time autocorrelation function of the unit vector directed from the branch point to the end of three arms for $B(B_3)_3$, and end-to-end vector for linear B_4 and linear B_7.

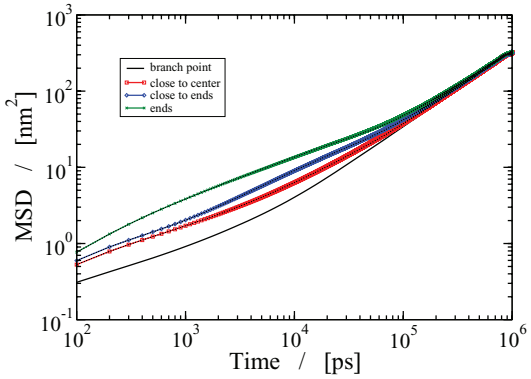

FIG. 9. Mean square displacement of each blob in $B(B_3)_3$ with entanglement. From the bottom to top, the curves are corresponding to the from innermost branch point to outermost free ends along each star arms.

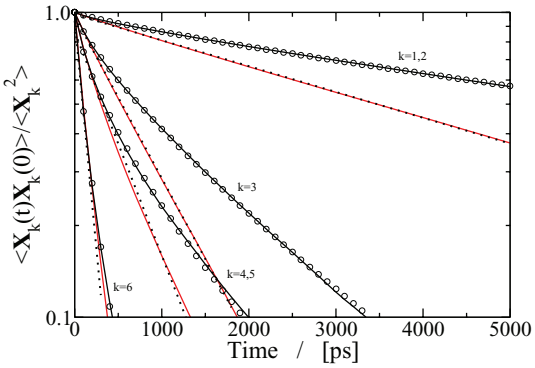

FIG. 10. Mode relaxations in $B(B_3)_3$, scaled as $\ln[C_k(t)]$ on a linear scale. The solid black and red curves are the modes corresponding to the system with and without entanglements. The circles and dotted lines are the respective fits for each mode number k.

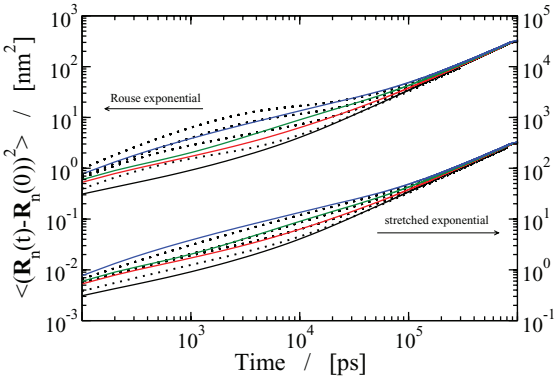

FIG. 11. Blob displacements of $B(B_3)_3$. The dotted lines are numerical calculations from the modes: the upper groups are using the Rouse exponential fit, and the lower groups are the ones from stretched exponential fit. The solid lines are simulation results for comparisons.

Appendix amounts to a transformation from blob-coordinates $\mathbf{R}_k$ to Rouse coordinates $\mathbf{X}_k$ which are chosen such that the coupled motion of the blobs in the Rouse model becomes decoupled. The time correlation functions of the Rouse coordinates, Rouse mode correlation functions for short, within the Rouse model decay exponentially with relaxation times τ_k. In case the Rouse model does not apply, the Rouse coordinates still provide interesting coordinates to describe the motion of the blobs, in particular to reveal deviations from Rouse behavior. Due to interactions between non-bonded blobs and the uncrossability constrains, the Rouse mode time correlation functions will not follow the exponential decay, and may usually be described reasonably well by the so-called stretched exponentials according to

$$C_k(t) = \langle(\mathbf{X}_k(t)\cdot\mathbf{X}_k(0))\rangle/\langle\mathbf{X}_k^2\rangle = \exp[-(t/\tau_k^*)^{\beta_k}], \qquad (13)$$

the relaxation time τ_k^* and stretching parameter β_k are obtained for each Rouse mode number k by fitting Eq. (13) to the simulated normalized Rouse mode autocorrelation $C_k(t)$. Notice that β_k is equal to one in case the Rouse model applies.

In Fig. 10, we have plotted $C_k(t)$ both for simulations with and without taking entanglements into account. For all modes, the unentangled Rouse mode correlations are perfectly well described by simple exponentially decaying functions, indicating that the soft potential Eq. (5) does not lead to non-Rouse behavior. Moreover, at very short times, the Rouse mode correlation functions of the entangled and non-entangled simulations are tangential to each other. Quickly, however, entanglements severely slow down the Rouse mode correlations such that they cannot be described anymore by simple exponentials, although the stretched exponentials of Eq. (13) still do a very good job.

According to Eq. (A12), the blob positions can be calculated from the Rouse mode coordinates. Assuming that in the real system Rouse modes are still not correlated, blob mean square displacements may be calculated according to

$$\langle[\mathbf{R}_n(t)-\mathbf{R}_n(0)]^2\rangle = 6D_R t + 2\sum_{k=1}^{N-1} S_{nk}^2\langle\mathbf{X}_k\cdot\mathbf{X}_k\rangle(1-C_k(t)). \qquad (14)$$

In Fig. 11, the solid curves are the blob displacements calculated from the simulation. The dotted lines are calculated according to Eq. (14) using the simulated diffusion coefficient D_R and the exponential representation of the Rouse mode correlation functions (upper group of curves, left vertical axis) or the stretched exponential representation of the Rouse mode correlation functions (lower group of curves, right vertical axis). It is clearly seen that the Rouse model representation, i.e., the exponential representation of the Rouse mode correlation functions, leads to blob motions much faster than the actual motions, while the stretched exponential representation gives almost correct results. The remaining deviations in the latter case may be caused by correlations between different Rouse modes, or by small deviations of the Rouse mode correlation functions from their stretched exponential fits.

We now turn our attention to the viscoelastic properties of our star polymer $B(B_3)_3$ melt. In Fig. 12, the storage and loss moduli, $G'(\omega)$ and $G''(\omega)$, are plotted as a function of frequency. Both curves are calculated as the appropriate Fourier transform of the stress relaxation modulus $G(t)$, shown in the inset. In the low frequency region, $G'(\omega)$ and $G''(\omega)$ are proportional to ω and ω^2, respectively. The crossing of both curves occurs when ω approximately equals 10^{-3}/ps, which means that the longest relaxation time of $B(B_3)_3$ is roughly equal $t = \omega^{-1} = 10^3$ ps. At frequencies beyond the

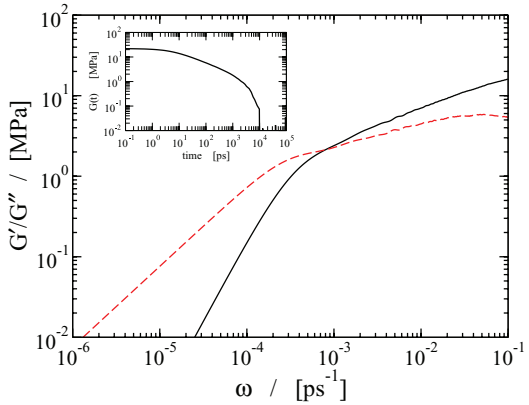

FIG. 12. The storage and loss moduli, $G'(\omega)$ and $G''(\omega)$, of $B(B_3)_3$ system, transformed from stress relaxation curve $G(t)$ on top left.

crossing point, $G'(\omega)$ becomes larger than $G''(\omega)$, and both curves continue to increase up to the highest frequency that can be investigated with the present coarse-grain model. The continuous increase of the loss modulus after crossing the storage modulus is in agreement with experimental[4] and theoretical[2,3] predictions for small stars. Since our star is rather short, the slope of the loss modulus is still rather large. Only for very large stars will the slope practically become zero; this holds true both for Rouse stars as well as for entangled stars.

B. Comparisons between star and linear polymers

Segmental motions in general reveal (part of) the topological constraints in complex polymers. In order to better understand the relation between topological constraints and architectural complexity, we compare the conformational and dynamical properties of $B(B_3)_3$ and those of related linear chains. We selected three linear chains for comparison: B_4, which corresponds to the length of one arm, B_7, which corresponds to the longest linear backbone in $B(B_3)_3$ between two ends, and B_{10}, corresponding to a linear chain having the same number of blobs or molecular weight as the target star.

The radius of gyration R_g can be calculated directly from the simulated configurations, or assuming Rouse-like behavior and using

$$R_g = \sqrt{\frac{1}{N}\sum_{k=1}^{N-1}\langle \mathbf{X}_k \cdot \mathbf{X}_k \rangle} = b\sqrt{\frac{1}{N}\sum_{k=1}^{N-1}\frac{1}{\lambda_k}}, \qquad (15)$$

where b is the Kuhn length and λ_ks are the eigenvalues of the connectivity matrix T (see the Appendix). The value of R_g^2 for $B(B_3)_3$ is 4.065 nm^2, and the ratio of R_g^2 of $B(B_3)_3$ to that of B_{10} turns out to be 0.86, which is a bit larger than the theoretical or experimental value 0.8[48,49] obtained with very large molecular weights.

It is interesting to compare the branch-end vector autocorrelation function of the star arms with the end-end vector autocorrelation functions of various linear chains as shown in Fig. 7. As is to be expected, the star arms relax much slower than the corresponding linear chain B_4. The slowing down effect of connecting three arms together is actually so strong that the arm relaxation is even much slower than the end-end vector relaxation of the longest chain present in the star, i.e., B_7.

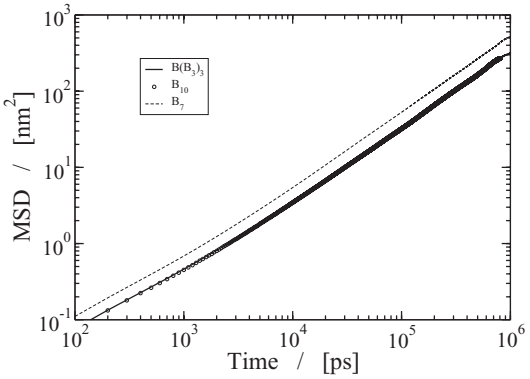

FIG. 13. Comparisons of center of mass mean square displacement in $B(B_3)_3$, B_{10}, and B_7.

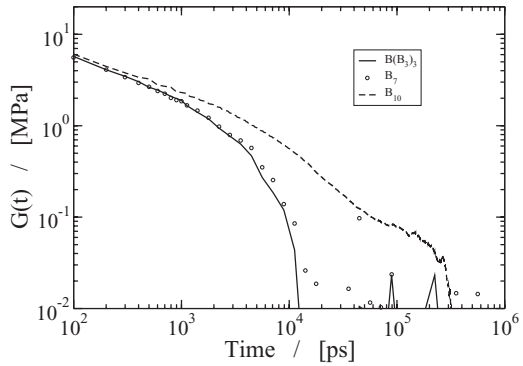

FIG. 14. Comparisons of zero shear relaxation in $B(B_3)_3$, B_{10}, and B_7.

We next compare star and linear chains by their center of mass mean square displacements and zero shear relaxation moduli. Fig. 13 reveals that the MSD curve of $B(B_3)_3$ (solid line) strongly overlaps with the one of B_{10} (circle symbol) and is substantially slower than that of B_7. Notice that our linear stars are too small to show the various regimes in the (blob-) mean square displacements that are so characteristic for reptational motion. In fact, our longest chain is a bit shorter than two entanglement lengths. We refer to the original papers of Padding and Briels for further information on this issue.[26] Although somewhat boldly, we conclude/surmise that relatively small stars diffuse similar to linear polymers of equal mass; on the basis of the present results, nothing can be said about the diffusive behavior of much larger stars.

In contrast, Fig. 14 shows that the stress relaxation of $B(B_3)_3$ is much faster than that of B_{10}, very akin to that of B_7. Intuitively, one may say that stress fluctuations are roughly proportional to the largest distance between two points of applied forces. These are very similar in $B(B_3)_3$ and B_7, and substantially shorter than in B_{10}. By integrating G(t), we have calculated zero shear rate viscosities, finding $\eta_0(B_7) = 9.22 \times 10^{-3}$ Pa s, $\eta_0(B_{10}) = 32.3 \times 10^{-3}$ Pa s, and $\eta_0(B(B_3)_3) = 9.19 \times 10^{-3}$ Pa s. For the two linear polymers, these results are in agreement with those in Ref. 26, and in good agreement with experiments. We could not compare the star polymer to experimental results, because synthesized stars typically have much larger arms.

IV. CONCLUSIONS

In this work, the TWENTANGLEMENT code to perform coarse-grain simulations of linear polymers has been made applicable to polymers of more complex architectures. In order to deal with complex architectures we have included the possibility to connect several polymers at one branch point (of course, one complex polymer may contain more than one branch point). We have tested our code by connecting two linear chains into a longer linear chain. Next, we applied our method to build a star polymer $B(B_3)_3$ and investigated its dynamical and rheological properties. The results were compared with those of linear melts with molecular weight equal to that of the entire molecule or that of the main back bone

chain consisting of two arms and the branch point of our three-arm star.

From our simulations, we found that the shape of the polymer has an important effect on the properties of the melt. We observed different dynamics for different star polymer segments. Rouse mode correlation functions could be well described by stretched exponentials. Assuming uncorrelated Rouse modes we recovered the blob mean square displacements almost completely, meaning that different Rouse modes are only slightly correlated. The comparison with linear chains revealed that (relatively short) star polymers diffuse as linear chains of equal mass, whereas they display rheological behavior very similar to that of the linear polymer with a molecular mass equal to that of the longest linear chain available in the star.

Obviously, each arm of our $B(B_3)_3$ represents a rather short polymer, approximately a bit less than one entanglement length, but still long enough to capture some characteristics of a star polymer melt that is different from a linear polymer melt. Future work will focus on simulations of stars having longer entangled arms and different numbers of arms to understand the chain length and branching degree effect. Efforts are also in progress aiming at simulating branched polymers of other shapes.

ACKNOWLEDGMENTS

The research leading to these results has received funding from the [European Community's] Seventh Framework Programme [FP7/2007-2013] under Grant Agreement No. 214627-DYNACOP. The authors thank SoftComp for computer time.

APPENDIX: ROUSE MODEL OF NONLINEAR POLYMERS

In this Appendix, we quickly review the salient features of the Rouse model as applied to nonlinear polymers. We collect all position vectors $\mathbf{R}_n$ in one long vector R. To be clear, every entry of R is a vector, not one of its Cartesian coordinates. The total number of entries in R is therefore equal to the number of blobs N in each polymer. The equation of motion then reads

$$\frac{dR}{dt} = -wTR + F, \tag{A1}$$

here T is a symmetric matrix reflecting the topology of the polymer and F is a vector of random displacements, for which

$$\begin{aligned} \langle F(t)\rangle &= 0, \\ \langle F(t)\cdot F(0)^T\rangle &= 6D\mathbb{I}\delta(t), \end{aligned} \tag{A2}$$

Here, $\mathbb{I}$ denotes the $N\times N$ unit matrix. Finally, w denotes the elementary Rouse rate and $D=\frac{1}{3}b^2w$ with b being the Kuhn length.

As an example, we mention that equations of motion for the smallest possible three arm star BB_3 read as

$$\begin{aligned} \frac{d\mathbf{R}_0}{dt} &= -w(3\mathbf{R}_0-\mathbf{R}_1-\mathbf{R}_2-\mathbf{R}_3)+\mathbf{f}_0, \\ \frac{d\mathbf{R}_1}{dt} &= -w(\mathbf{R}_1-\mathbf{R}_0)+\mathbf{f}_1, \\ \frac{d\mathbf{R}_2}{dt} &= -w(\mathbf{R_2}-\mathbf{R_0})+\mathbf{f_2}, \\ \frac{d\mathbf{R}_3}{dt} &= -w(\mathbf{R}_3-\mathbf{R}_0)+\mathbf{f}_3, \end{aligned} \tag{A3}$$

from which we see that the matrix T reads

$$T=\begin{bmatrix} 3 & -1 & -1 & -1 \\ -1 & 1 & 0 & 0 \\ -1 & 0 & 1 & 0 \\ -1 & 0 & 0 & 1 \end{bmatrix}. \tag{A4}$$

Likewise for $B(B_3)_3$, we find

$$T=\begin{bmatrix} 3 & -1 & 0 & 0 & -1 & 0 & 0 & -1 & 0 & 0 \\ -1 & 2 & -1 & 0 & 0 & 0 & 0 & 0 & 0 & 0 \\ 0 & -1 & 2 & -1 & 0 & 0 & 0 & 0 & 0 & 0 \\ 0 & 0 & -1 & 1 & 0 & 0 & 0 & 0 & 0 & 0 \\ -1 & 0 & 0 & 0 & 2 & -1 & 0 & 0 & 0 & 0 \\ 0 & 0 & 0 & 0 & -1 & 2 & -1 & 0 & 0 & 0 \\ 0 & 0 & 0 & 0 & 0 & -1 & 1 & 0 & 0 & 0 \\ -1 & 0 & 0 & 0 & 0 & 0 & 0 & 2 & -1 & 0 \\ 0 & 0 & 0 & 0 & 0 & 0 & 0 & -1 & 2 & -1 \\ 0 & 0 & 0 & 0 & 0 & 0 & 0 & 0 & -1 & 1 \end{bmatrix}. \tag{A5}$$

We solve Eq. (A1) by diagonalizing matrix T,

$$\begin{aligned} R &= SX, \\ \frac{dX}{dt} &= -w\Lambda X + G, \\ \Lambda &= S^{-1}TS, \\ G &= S^{-1}F, \end{aligned} \tag{A6}$$

here S is chosen such that Λ is diagonal, i.e., such that the columns of S are mutually orthogonal eigenvectors of T. The entries of X are called Rouse vectors. It is convenient to normalize these eigenvectors to unity, in which case $S^{-1}=S^T$. In that case,

$$\begin{aligned} \langle G\rangle &= 0, \\ \langle G(t)\cdot G(0)^T\rangle &= 6D\mathbb{I}\delta(t). \end{aligned} \tag{A7}$$

Always one of the eigenvalues of T is equal to zero, with corresponding normalized eigenvector having all entries equal to $1/N$. The corresponding Rouse-vector $\mathbf{X}_0$ and random

displacement vector $\mathbf{G}_0$ are given by

$$\mathbf{X}_0 = \frac{1}{\sqrt{N}}\sum_{k=1}^{N}\mathbf{R}_k,$$
$$\mathbf{G}_0 = \frac{1}{\sqrt{N}}\sum_{k=1}^{N}\mathbf{F}_k. \tag{A8}$$

Solving the equation of motion in this case, we find

$$\mathbf{X}_0(t) = \mathbf{X}_0(0) + \int_0^t dt'\mathbf{G}_0(t'),$$
$$\langle[\mathbf{X}_0(t) - \mathbf{X}_0(0)]^2\rangle = 6Dt. \tag{A9}$$

Notice that $\mathbf{X}_0$ is $\sqrt{N}\mathbf{R}_{cm}$, so the diffusion coefficient is $D_R = D/N$.

For the Rouse-vectors with non-zero eigenvalues, we obtain

$$\mathbf{X}_k(t) = \mathbf{X}_0(0)e^{-w\lambda_k t} + \int_0^t dt' e^{-w\lambda_k(t-t')}\mathbf{G}_k(t'). \tag{A10}$$

Noticing that $\langle\mathbf{X}_k(t)\cdot\mathbf{X}_k(t)\rangle = \langle\mathbf{X}_k(0)\cdot\mathbf{X}_k(0)\rangle$, we find

$$\langle\mathbf{X}_k\cdot\mathbf{X}_k\rangle = 6D/(2w\lambda_k) = b^2/\lambda_k,$$
$$\langle[\mathbf{X}_k(t) - \mathbf{X}_k(0)]^2\rangle = \frac{2b^2}{\lambda_k}(1 - e^{-w\lambda_k t}), \tag{A11}$$

with these results we are now in the position to calculate blob mean square displacements. For this purpose, notice that

$$\mathbf{R}_n = \frac{1}{\sqrt{N}}\mathbf{X}_0 + \sum_{k=1}^{N-1} S_{nk}\mathbf{X}_k. \tag{A12}$$

We then easily obtain

$$\langle[\mathbf{R}_n(t) - \mathbf{R}_n(0)]^2\rangle$$
$$= 6D_R t + 2\sum_{k=1}^{N-1} S_{nk}^2\langle\mathbf{X}_k\cdot\mathbf{X}_k\rangle(1 - e^{-\omega\lambda_k t}). \tag{A13}$$

The example of BB_3 given above has eigenvalues $\lambda_k = 0$, 1, 1, 4. The corresponding S-matrix reads

$$S = \begin{bmatrix} \frac{1}{2} & 0 & 0 & \frac{1}{2}\sqrt{3} \\ \frac{1}{2} & \frac{1}{2}\sqrt{2} & 0 & 0 \\ \frac{1}{2} & -\frac{1}{2}\sqrt{2} & 1 & 0 \\ \frac{1}{2} & 0 & 0 & 1 \end{bmatrix}. \tag{A14}$$

Similarly, the S for $B(B_3)_3$ can be calculated.

[1]M. P. Cornelia Vasile, *Practical Guide to Polyethylene* (Rapra Technology Limited, 2005).
[2]D. S. Pearson and E. Helfand, Macromolecules **17**, 888 (1984).
[3]T. C. B. McLeish and S. T. Milner, Adv. Polym. Sci. **143**, 195 (1999).
[4]L. J. Fetters, A. D. Kiss, and D. S. Pearson, Macromolecules **26**, 647 (1993).
[5]W. W. Graessley and J. Roovers, Macromolecules **12**, 959 (1979).
[6]Z. Wang, X. Chen, and R. G. Larson, J. Rheol. **54**, 223 (2010).
[7]W. Pyckhout-Hintzen, J. Allgaier, and D. Richter, Eur. Polym. J. **47**, 474 (2011).
[8]D. J. Lohse, S. T. Milner, L. J. Fetters, and M. Xenidou, Macromolecules **35**, 3066 (2002).
[9]A. Jabbarzadeh, J. D. Atkinson, and R. I. Tanner, Macromolecules **36**, 5020 (2003).
[10]N. C. Karayiannis and V. G. Mavrantzas, Macromolecules **38**, 8583 (2005).
[11]K. Hur, C. Jeong, R. G. Winkler, N. Lacevic, R. H. Hee, and D. Y. Yoon, Macromolecules **44**, 2311 (2011).
[12]J. Liu, W. Yu, and C. Zhou, J. Rheol. **55**, 545 (2011).
[13]P. E. Rouse, J. Chem. Phys. **21**, 1272 (1953).
[14]M. Doi and S. F. Edwards, *The Theory of Polymer Dynamics* (Clarendon, Oxford, 1986).
[15]D. S. Pearson, G. V. Strate, E. V. Meerwall, and F. C. Schilling, Macromolecules **20**, 1133 (1987).
[16]C. B. Gell, W. W. Graessley, and L. J. Fetters, J. Polym. Sci., Part B: Polym. Phys. **35**, 1933 (1997).
[17]S. Q. Wang, J. Polym. Sci., Part B: Polym. Phys. **41**, 1589 (2003).
[18]V. A. Harmandaris, V. G. Mavrantzas, and D. N. Theodorou, Macromolecules **31**, 7934 (1998).
[19]J. D. Moore, S. T. Cui, H. D. Cochran, and P. T. Cummings, J. Non-Newtonian Fluid Mech. **93**, 83 (2000).
[20]W. Paul, G. D. Smith, and D. Y. Yoon, Macromolecules **30**, 7772 (1997).
[21]C. Baig, O. Alexiadis, and V. G. Mavrantzas, Macromolecules **43**, 986 (2010).
[22]V. A. Harmandaris, V. G. Mavrantzas, D. N. Theodorou, M. Kröger, J. Ramírez, H. C. Öttinger, and D. Vlassopoulos, Macromolecules **36**, 1376 (2003).
[23]F. Müller-Plathe, Chem. Phys. Chem. **3**, 754 (2002).
[24]T. Strauch, L. Yelash, and W. Paul, Phys. Chem. Chem. Phys. **11**, 1942 (2009).
[25]J. T. Padding and W. J. Briels, J. Chem. Phys. **115**, 2846 (2001).
[26]J. T. Padding and W. J. Briels, J. Chem. Phys. **117**, 925 (2002).
[27]Y. Zhu, H. Liu, and Z. Lu, J. Chem. Phys. **136**, 144903 (2012).
[28]J. T. Padding and W. J. Briels, J. Phys. Condens. Matter **23**, 233101 (2011).
[29]M. Zamponi, W. Pyckhout-Hintzen, A. Wischnewski, M. Monkenbusch, L. Willner, G. Kali, and D. Richter, Macromolecules **43**, 518 (2010).
[30]T. Cherdhirankorn, G. Floudas, H. J. Butt, and K. Koynov, Macromolecules **42**, 9183 (2009).
[31]C. R. Bartels, J. B. Crist, L. J. Fetters, and W. W. Graessley, Macromolecules **19**, 785 (1986).
[32]S. T. Milner and T. C. B. McLeish, Macromolecules **31**, 7479 (1998).
[33]C. H. Adams, L. R. Hutchings, P. G. Klein, T. C. B. McLeish, and R. W. Richards, Macromolecules **29**, 5717 (1996).
[34]S. T. Milner and T. C. B. McLeish, Macromolecules **30**, 2159 (1997).
[35]G. Ianniruberto and G. Marrucci, Macromolecules **46**, 267 (2013).
[36]Y. Masubuchi, G. Ianniruberto, F. Greco, and G. Marrucci, J. Chem. Phys. **119**, 6925 (2003).
[37]Y. Masubuchi, J. Takimoto, K. Koyama, G. Ianniruberto, G. Marrucci, and F. Greco, J. Chem. Phys. **115**, 4387 (2001).
[38]C. C. Hua and J. D. Schieber, J. Chem. Phys. **109**, 10018 (1998).
[39]D. M. Nair and J. D. Schieber, Macromolecules **39**, 3386 (2006).
[40]A. E. Likhtman, Macromolecules **38**, 6128 (2005).
[41]R. S. Graham, A. E. Likhtman, T. C. B. McLeish, and S. T. Milner, J. Rheol. **47**, 1171 (2003).
[42]A. E. Likhtman, S. T. Milner, and T. C. B. McLeish, Phys. Rev. Lett. **85**, 4550 (2000).
[43]A. van den Noort and W. J. Briels, J. Non-Newtonian Fluid Mech. **152**, 148 (2008).
[44]P. Kindt and W. J. Briels, J. Chem. Phys. **127**, 134901 (2007).
[45]J. T. Padding, L. V. Mohite, D. Auhl, W. J. Briels, and C. Bailly, Soft Matter **7**, 5036 (2011).
[46]W. J. Briels, Soft Matter **5**, 4401 (2009).
[47]I. S. Santos de Oliveira, A. van den Noort, J. T. Padding, W. K. den Otter, and W. J. Briels, J. Chem. Phys. **135**, 104902 (2011).
[48]B. H. Zimm and W. H. Stockmayer, J. Chem. Phys. **17**, 1301 (1949).
[49]N. Hadjichristidis *et al.*, Macromolecules **33**, 2424 (2000).